Nanoscopic Quantification of Sub-mitochondrial Morphology, Mitophagy and Mitochondrial Dynamics in Patients With Mitochondrial Disease

Weiwei Zou
Cincinnati Children's Hospital Medical Center Division of Human Genetics
Qixin Chen
Shandong First Medical University
Jesse Slone
University at Buffalo Jacobs School of Medicine and Biomedical Sciences: University at Buffalo School of Medicine and Biomedical Sciences
Li Yang
Xiangya Hospital Central South University
Xiaoting Lou
Wenzhou Medical University
Jiajie Diao
University of Cincinnati College of Medicine
Taosheng Huang (thuang29@buffalo.edu)
Division of Human Genetics, Cincinnati Children's Hospital Medical Center, 3333 Burnet Avenue, Cincinnati, OH 45229, USA https://orcid.org/0000-0001-6601-6687

Research

Keywords: nanoscope, mitochondrial disease, SLC25A46, cristae, mitophagy

Posted Date: November 17th, 2020

DOI: https://doi.org/10.21203/rs.3.rs-105738/v1

Abstract

SLC25A46 mutations have been found to lead to mitochondrial hyper-fusion and reduced mitochondrial respiratory function, which results in optic atrophy, cerebellar atrophy, and other clinical symptoms of mitochondrial disease. However, it is generally believed that mitochondrial fusion is attributable to increased mitochondrial oxidative phosphorylation (OXPHOS)[1], which is inconsistent with the decreased OXPHOS of highly-fused mitochondria observed in previous studies. In this paper, we have used the live-cell nanoscope to observe and quantify the structure of mitochondrial cristae, and the behavior of mitochondria and lysosomes in patient-derived *SLC25A46* mutant fibroblasts. The results show that the crista have been markedly damaged in the mutant fibroblasts, but that there is no corresponding increase in mitophagy. This study suggests that severely damaged mitochondrial cristae might be the predominant cause of reduced OXPHOS in *SLC25A46* mutant fibroblasts. This study demonstrates the utility of nanoscope-based imaging for realizing the sub-mitochondrial morphology, mitophagy and mitochondrial dynamics in live cells, which may be particularly helpful for the quick assessment and diagnosis of mitochondrial abnormalities.

Background

The mitochondron is the cellular organelle which is most intimately associated with energy metabolism in mammals and most other eukaryotes. Mitochondrial dysfunction caused by nuclear DNA (nDNA) or mitochondrial DNA (mtDNA) defects lead to cellular respiratory chain and energy metabolism disorders, resulting in a group of multi-system diseases [1, 2]. A number of mitochondrial diseases present aberrant mitochondrial morphology, including mitochondrial fragmentation or excessive mitochondrial fusion, which have an effect on mitochondrial function, leading to dysfunction of vital organs and tissues and accordingly threatening patients' health and survival [3–5].

The confocal microscope and transmission electron microscope are commonly used to observe mitochondrial morphology. However, a major shortcoming of the confocal microscope is that its spatial resolution is not high enough to visualize and quantitatively calculate the structure of sub-mitochondria, which is vital for examining the sub-mitochondrial damage that may affect mitochondrial function [6]. Transmission electron microscopy, however, is time-consuming, expensive, and unable to observe the variations of live-cell mitochondrial morphology in a dynamic manner. The spatial resolution of 100–120 nm achieved by the structured illumination microscopy (SIM) is sufficient to observe the sub-mitochondrial structure in living cells [7].

In this paper, we have set out to take advantage of the live-cell nanoscope − 3D-SIM to dynamically observe the sub-mitochondrial morphology originating from the fibroblasts of a patient carrying biallelic mutations in *SLC25A46*. Combined with the sub-mitochondrial structure identification/quantification and mitochondria-lysosome interaction quantification methods developed by our group [8–11], we have used this approach to identify and quantify the mitochondrial internal structure (cristae) and mitochondrial-

lysosomal interaction of live cells. We consequently provide a new method for the identification of the mechanisms of mitochondrial oxidative phosphorylation (OXPHOS) dysfunction.

Results

The reduced metabolic ability of patient-derived SLC24A46 mutant fibroblasts

The mitochondrial respiration function was investigated by examining OCR under both basal conditions and drug-induced mitochondrial stress using the Seahorse assay. The OCR was found to be significantly decreased in patient-derived *SLC25A46* mutant fibroblasts compared to normal fibroblasts (Fig. 1A). After a detailed analysis, the basal respiration, oxygen consumption for ATP production, maximum oxygen consumption capacity of mitochondria, proton-leaked oxygen consumption, non-mitochondrial respiration, and the spare respiratory capacity in patient-derived *SLC25A46* mutant fibroblasts were all lower than that of normal fibroblasts (Fig. 1B).

The MTT assay reflects the metabolic ability of living cells by measuring the proliferation rates of cells. The results of this assay for the mutant and normal fibroblasts showed no apparent difference in the number of living cells between these two types of fibroblasts on Day 2 after cell seeding. However, subsequent to this time point, the normal fibroblasts showed vigorous metabolism and rapid proliferation rate on Day 4, Day 6, and Day 8 (Fig. 1D). Thus, the metabolic ability and cell proliferation rate of *SLC25A46* mutant fibroblasts were significantly lower than that of normal fibroblasts (Fig. 1D). The imaging results showed that the cell density of normal fibroblasts was close to 80–90% on Day 8, while it only reached 40–50% in *SLC25A46* mutant fibroblasts (Fig. 1C).

Mitochondrial hyper-fusion in patient-derived SLC24A46 mutant fibroblasts with the live-cell nanoscope-3D-SIM imaging system

The decreased metabolic ability of mutant fibroblasts suggested that the mitochondrial function in *SLC25A46* mutant fibroblasts has been disturbed. Sanger sequencing results showed a homozygous, missense point mutation (c.1005A > T; p. Glu335Asp) in *SLC25A46* mutant fibroblasts (Fig. 2D). To examine whether this mutation causes any changes in mitochondrial morphology, we used a nanoscope – 3D-SIM imaging approach to observe mitochondrial morphology in those two human cells. The images showed that the normal fibroblasts had round or medium length mitochondria (Fig. 2A), while the *SLC25A46* mutant fibroblasts showed slender, hyper-fused mitochondria (Fig. 2B). Imaris software (Nikon, Tokyo, Japan) was used to identify and analyze the mitochondria morphology (Fig. 2C). The results showed that the number of mitochondria in *SLC25A46* mutant fibroblasts was significantly lower than what was observed in normal fibroblasts. In contrast, the average area and volume of mitochondria in mutant cells were significantly greater than those in normal fibroblasts (Fig. 2E). The comparative analysis of mitochondrial morphology showed aberrant hyper fusion of mitochondria in the patient-derived *SLC24A46* mutant fibroblasts.

Severe damage of mitochondrial cristae in patient-derived SLC24A46 mutant fibroblasts

Previously, mitochondrial fusion was considered to facilitate OXPHOS, and an increase of mitochondrial fusion will improve the mitochondrial OXPHOS level [12, 13]. Mediated mitochondrial fusion was therefore regarded as a new therapeutic target for mitochondrial diseases [14, 15]. However, our group found that the highly-fused mitochondria from *SLC25A46* mutant fibroblasts resulted in reduced OXPHOS [16]. What is the underlying cause of this rare condition? One possibility is alterations in the cristae, a most important structures of the inner mitochondrial membrane (IMM), which are deemed as the core of ATP production and mitochondrial respiratory function [17, 18]. Therefore, we decided to investigate whether structural defects of mitochondrial cristae lead to decreased OXPHOS.

Using algorithm-based SIM imaging technology previously developed by our team [8], we identified and extracted cristae first, then quantitatively analyzed the mitochondrial cristae for human-derived normal and patient-derived *SLC25A46* mutant fibroblasts. The images showed that the mitochondrial cristae structure was visible and abundant in normal fibroblasts (Fig. 3A). In contrast, the cristae structure was damaged or even vanished in *SLC25A46* mutant fibroblasts (Fig. 3B). After quantification analysis, the mean cristae number (Fig. 3C), cristae length (Fig. 3D), and cristae area (Fig. 3E) of *SLC25A46* mutant fibroblasts all showed a significant lower values than those observed in normal fibroblasts.

A similar tendency of mitophagy was observed in normal and SLC25A46 mutant fibroblasts

Mitophagy is the general process by which the cell removes severely damaged mitochondria, consequently achieving the purpose of “quality control” of mitochondria within living cells [19, 20]. We observed highly-fused mitochondria with severely damaged cristae structures in *SLC25A46* mutant fibroblasts. This raised the obvious questions of whether or not these abnormal mitochondria induce mitophagy? Using the SIM image-based mitochondria-lysosome co-location analysis method in living cells [9], we can observe and quantify mitophagy in normal and *SLC25A46* mutant fibroblasts (Fig. 4C).

Our results demonstrate that only slight levels of mitophagy are occurring in both of these cell lines (Fig. 4A, Fig. 4B). After quantitative analysis, there was no statistically significant difference in the value of mitochondrial - lysosome co-location between the two cell lines. Western Blot also confirmed that the values of the LC3-II/LC3-I ratio were comparable between normal and *SLC25A46* mutant fibroblasts (Fig. 4d), which was consistent with the results of the SIM image-based analysis method. In addition, with this nanoscope, we can straightforwardly monitor the mitochondrial dynamics and the mitochondria – lysosome interaction dynamics (Fig. 4e).

This novel nanoscope combined with a quantification analysis strategy can not only be used to observe mitochondrial morphology, but also to detect and quantify the damage of structures in sub-mitochondria, assess the extent of mitophagy, and monitor the dynamics of mitochondria and lysosome (Fig. 5). Therefore, this novel approach is a great approach for the observation and etiological diagnosis of mitochondrial damage in patients with mitochondrial disease.

Discussion

SLC25A46 is responsible for encoding a mitochondrial solute carrier protein [21]. We identified SLC25A46 is the human homolog of Ugo1, a protein of *Saccharomyces cerevisiae* and located in the mitochondrial outer membrane and involved in mitochondrial fusion [16, 22, 23]. So far, SLC25A46 has been found to be associated with various human diseases. Homozygous or compound heterozygous mutations of *SLC25A46* led to a range of clinical syndromes, with the clinical feature of optic atrophy, cerebellar atrophy, progressive myoclonic ataxia, axonal peripheral neuropathy, autosomal recessive cerebellar ataxias (ARCA), lethal congenital pontocerebellar hypoplasia, and even Parkinson's disease [16, 21, 24–29]. Mice with *Slc25a46* dysfunction developed severe motor impairment, optic atrophy, and developmental defects of the nervous system, as well as premature death [30–32].

Currently, SLC25A46 is believed to affect mitochondrial dynamics due to the interaction with OPA1 and MFN2 [33, 34]. The hyper-fused mitochondria and reduced mitochondrial respiratory function presented in patient-derived *SLC25A46* mutant fibroblasts have also been confirmed by this study, as well as previous studies, which was supposed to be the pathogenic mechanism of a series of neurological diseases [35]. The MTT assay results from this study also strengthened the idea that the metabolic capacity of *SLC25A46* mutant fibroblasts is significantly lower than that of control cells. However, there exists a contradiction between the morphology of highly-fused mitochondria and the decline of mitochondrial function. Traditionally, mitochondrial fusion has been verified to be vital for maintaining mtDNA stability and improving the tolerance of cells to high mtDNA mutations [36, 37]. At the same time, mitochondrial fusion is also a protective factor for maintaining normal mitochondrial respiration function. The absence of mitochondrial fusion in the cerebellum has also been shown to result in a malformed mitochondrial distribution and function [38]. Moreover, mitochondrial fusion is required to support the normal development of embryos [3]. Why then do the SLC25A46 mutant cells examined in our study show mitochondrial hyper-fusion, but a decrease in mitochondrial respiratory function?

The respiratory function of mitochondria is a series of oxidation-reduction reactions mediated by multiple complexes located on the mitochondrial inner cristae, which eventually produce ATP and provide energy for the tissues and cells in living organisms [39, 40]. From this viewpoint, we hypothesized that *SLC25A46* mutation causes structural abnormalities of cristae in highly fused mitochondria, consequently affecting mitochondrial respiratory function. Based on the identification and quantification method of mitochondrial cristae invented by our group, we analyzed the mitochondrial internal cristae of patient-derived *SCL25A46* mutant fibroblasts and human-derived normal fibroblasts. Our results showed that, compared with normal mitochondria, the number of mitochondrial cristae decreased, the length of cristae shortened, and the area of cristae was reduced in the *SLC25A46* mutant fibroblasts. We even observed the disappearance of cristae in some mitochondria. Therefore, we posited that the structure of mitochondrial cristae in the mutant cells was damaged, which accordingly affected the mitochondrial respiratory function, as reflected by decreased aerobic respiration, reduced ATP generation and decreased metabolic capacity. Researchers have suggested that SLC25A46 plays a vital role in the interaction between the major structural proteins of the mitochondrial outer membrane and the mitochondrial cristae, and it is crucial for maintaining the structure and stability of the mitochondrial cristae. Immunoblot analysis revealed that MIC60 and MIC19 – two critical proteins of mitochondrial contact site and cristae

organizing system (MICOS) complex obviously decreased in patient-derived *SLC25A46* mutant fibroblast. And immunoprecipitation experiments showed SLC25A46 co-immunoprecipitated with MIC60, MIC19, OPA1 (located on IMM), MFN1 and MFN2 (located on OMM) [33]. MICOS complex, especially MIC60 and MIC19, is a crucial factor in cristae biogenesis [41, 42]. Therefore, SLC25A46 is believed to be not only involved in maintaining the stability of OMM, but also an essential protein in the interaction and communication between the OMM and IMM, as well as the formation and maintenance of mitochondrial cristae [33]. They have used transmission electron microscopy and observed the significantly decreased cristae number and length from the patient-derived mitochondria [33]. This result from transmission electron microscopy is consistent with our nanoscope-based results.

Mitophagy is a crucial step in mitochondrial quality control, which is used to remove damaged mitochondria [43, 44]. Severe injury of mitochondrial cristae can induce mitophagy as well [45, 46]. Therefore, we also hypothesized that the damaged mitochondrial cristae would increase the rate of mitophagy in *SLC25A46* mutant fibroblasts. We monitored the dynamic changes of mitochondrial and lysosomal behavior in *SLC25A46* mutant fibroblasts in real-time. We observed a contact and co-localization phenomenon between lysosome and mitochondria after mitochondrial fragmentation in *SLC25A46* mutant fibroblasts. However, using the SIM image-based mitophagy quantification method we invented before, we determined that the overall tendency of mitophagy in the *SLC25A46* mutant fibroblasts was not statistically different from that in normal fibroblasts, although mitophagy did occur in some mitochondria in the *SLC25A46* mutant fibroblasts. Consequently, although the mitochondrial cristae were severely damaged in the *SLC25A46* mutant fibroblasts, the damaged cristae alone did not appear to induce the occurrence of mitophagy. Currently, no studies have reported the mitophagy status of *SLC25A46* mutant cells.

Conclusions

Overall, this study suggests that severely damaged mitochondrial cristae may be the predominant cause of reduced mitochondrial respiratory dysfunction in *SLC25A46* mutant fibroblasts, but that the damaged mitochondrial cristae do not induce a significant increase in mitophagy.

Through the usage of the SIM-based live-cell nanoscope and the quantification methods we developed, we can examine the morphology of the outer mitochondrial membrane (OMM), inner mitochondrial membrane (IMM), the rate of mitophagy, and also perform quantitative calculations of all these phenomena. Simultaneously, we can dynamically observe the behavior of mitochondria and lysosomes. We have thus achieved a comprehensive observation of mitochondrial morphology, internal structure, and mitophagy using a single technique. Therefore, this nanoscope is exceptionally suited for the observation and calculation of the mitochondria and sub-mitochondrial structures in live cells from patients with various mitochondrial diseases. The operation of the device is simple, rapid and accurate, which is helpful for the quick assessment and diagnosis of mitochondrial abnormalities.

Methods

Cell culture

The human-derived normal fibroblasts and patient-derived *SLC25A46* mutant (c.1005A > T, p.Glu335Asp) fibroblasts cell lines were acquired after informed consent was obtained from the patients. The cells were cultured in Dulbecco's modified Eagle's medium (DMEM) medium (Gibco, Thermo Fisher Scientific, USA) with 10% FBS (Gibco, Thermo Fisher Scientific, USA) and 100 units/ml Anti-Anti (containing streptomycin and penicillin) (Gibco, Thermo Fisher Scientific, USA) and incubated in a 5% CO2, 37℃ and 100% humidity incubator.

Nanoscope – 3D-SIM imaging

The cells were seeded in a glass-bottom culture dish (MatTek Life Sciences, USA) and cultured for 24 hours in 2 ml DMEM containing 10%FBS and 100 units/ml Anti-Anti. Before imaging, cells were first washed three times with a pre-warmed DMEM medium and then were incubated in a DMEM medium containing 100 nM Mito-Tracker Green (Invitrogen, USA) for half an hour. Cells for mitophagy analysis were co-incubated in DMEM medium containing 100 nM Mito-Tracker Green (Invitrogen, USA) and Lyso-Tracker Red (Invitrogen, USA) for half an hour. Cells were then washed three times with DMEM. The stained cells were photographed using the 3D-structure illumination microscope (Nikon, Tokyo, Japan).

Western blot

Protease inhibitor cocktail (Sigma, USA) and 2 × RIPA lysis and extraction buffer (Thermofisher Scientific, USA) were added to the centrifuged cell pellets, and then were sonicated for 5 minutes each time, three times in total. The protein concentration was measured by using the Pierce BCA Protein Assay Kit (Thermofisher Scientific, USA). 30ug protein for each sample and 4X NuPAGE LDS Sample Buffer (Thermofisher Scientific, USA) were mixed at 4:1 ratio and denatured at 95℃ for 5 minutes, and then separated in 4–12% Bis-Tris gel (Invitrogen, USA). The gel was transferred onto a PVDF membrane (Invitrogen, USA) through the iBlot 2 gel transfer device (Life Technologies, USA). The transferred PVDF membrane was placed in the Intercept Blocking Buffer (LI-COR Biosciences, USA) for 45 minutes, and then incubated overnight in the primary antibody, rabbit anti-LC3B (cell signaling technology, USA) diluted in the blocking buffer at a ratio of 1:200 with Tween 20 diluted in the blocking buffer at a ratio of 1:1000. Rabbit anti-GAPDH (cell signaling technology, USA) was also diluted in the blocking buffer at a ratio of 1:2000 and set as the loading control. The next day, the PVDF membrane was washed for 10 minutes each time, three times in total. Then, the membrane was incubated in the secondary antibody, IRDye 800CW Goat anti-Rabbit IgG (LI-COR Biosciences, USA), for 120 minutes. The bands were detected by the LI-COR Odyssey Clx Imaging System (LI-COR Biosciences, Lincoln, NE).

Sanger sequencing for mutation detection

To detect the point mutation of *SLC25A46* in human-derived normal and patient-derived fibroblasts, genomic DNA was extracted using DNeasy Blood & Tissue Kit (Qiagen, USA). PCR products of 186 bp in length were amplified using GoTag mater mixes (Promega, USA). The following primer set was used for the amplification: Forward: TGCCAGTCTTTGTTCTGACG and Reverse: CCAAACACTCCTTCCTCCTG. The

reactions were performed following the thermal cycling program: 95 °C for 2 minutes, followed by 30 cycles of 95 °C for 30 seconds, 56 °C for 30 seconds, and 72 °C for 30 seconds. A final extension step was then performed at 72 °C for 4 minutes.

Oxygen consumption rate (OCR) measurement

Human-derived normal and patient-derived *SLC25A46* mutant cells were seeded at a density of 1.0×10^4 cells/well with DMEM supplemented with 10% FBS in XFe96 cell culture plates (Agilent Technologies, USA). After incubation for 24 hours, the DMEM medium was removed and changed with the warmed XF DMEM Medium supplemented with 1 mM sodium pyruvate, 10 mM glucose and 2 mM L-glutamine at pH 7.4. All cells were treated with 1 μM oligomycin A, 1 μM FCCP, and 500 nM rotenone/antimycin A. The OCRs of the cells was assessed by using the XF Cell Mito Stress Test Kit (Agilent Technologies, USA). The Seahorse XF96 analyzer (Agilent Technologies, USA) was used for OCR measurement.

Cell proliferation rate measurement (MTT assay)

Human-derived normal and patient-derived *SLC25A46* mutant fibroblasts were seeded in 96 well plates (Corning, USA) at a density of 3.0×10^3 cells/well with DMEM supplemented with 10% FBS and incubated at 37˚C, 5% CO2. 10 μl of MTT solution (Roche, USA) was added to 100 ul culture medium in each well at a final concentration of 0.5 mg/ml. The following process was implemented according to the manual provided by the kit. The absorbance was detected at 570 nm by the microplate reader (BioTek, USA).

Statistical analysis

Graphpad Prism 7 software was used to display data. Independent-Samples T-test was used for statistical analysis. * was defined as $P < 0.05$, ** as $P < 0.01$, *** as $P < 0.001$, and **** as $P < 0.0001$.

Abbreviations

OXPHOS
oxidative phosphorylation
nDNA
nuclear DNA
mtDNA
mitochondrial DNA
SIM
structured illumination microscopy
OCR
Oxygen consumption rate
IMM
inner mitochondrial membrane
OMM
outer mitochondrial membrane

Declarations

Ethics approval and consent to participate

Informed consent was obtained from the patients before taking the samples. This study was approved by the Institutional Review Board of Cincinnati Children's Hospital Medical Center.

Consent for publication

Not applicable.

Availability of data and materials

The datasets used and/or analysed during the current study are available from the corresponding author on reasonable request.

Competing interests

The authors declare that they have no competing interests.

Funding

This work was supported by the Hadley J. Foundation and National Institute of Child Health & Development 1R01HD092989.

Authors' contributions

TH and JJ conceived the idea and designed the experiments. WZ, QC, YL, and XL carried out the experiments of the manuscript. WZ, QC, JS, and JD participated in the analysis and interpretation of the data. WZ prepared the figures and the original draft. QC, YL, and XL corrected the figures. TH, JJ, and JS reviewed and revised the manuscript. All authors read and approved the final manuscript.

Acknowledgements

Not applicable.

References

1. Craven L, Alston CL, Taylor RW, Turnbull DM. Recent Advances in Mitochondrial Disease. Annual review of genomics and human genetics. 2017;18:257-75.
2. Alston CL, Rocha MC, Lax NZ, Turnbull DM, Taylor RW. The genetics and pathology of mitochondrial disease. The Journal of pathology. 2017;241(2):236-50.
3. Chen H, Detmer SA, Ewald AJ, Griffin EE, Fraser SE, Chan DC. Mitofusins Mfn1 and Mfn2 coordinately regulate mitochondrial fusion and are essential for embryonic development. The

Journal of cell biology. 2003;160(2):189-200.
4. Reddy PH. Inhibitors of mitochondrial fission as a therapeutic strategy for diseases with oxidative stress and mitochondrial dysfunction. Journal of Alzheimer's disease : JAD. 2014;40(2):245-56.
5. Chan DC. Mitochondrial Dynamics and Its Involvement in Disease. Annual review of pathology. 2020;15:235-59.
6. Fang H, Yao S, Chen Q, Liu C, Cai Y, Geng S, et al. De Novo-Designed Near-Infrared Nanoaggregates for Super-Resolution Monitoring of Lysosomes in Cells, in Whole Organoids, and in Vivo. ACS nano. 2019;13(12):14426-36.
7. Qiu K, Du Y, Liu J, Guan JL, Chao H, Diao J. Super-resolution observation of lysosomal dynamics with fluorescent gold nanoparticles. Theranostics. 2020;10(13):6072-81.
8. Shao X, Chen Q, Hu L, Tian Z, Liu L, Liu F, et al. Super-resolution quantification of nanoscale damage to mitochondria in live cells. Nano Research. 2020;13(8):2149-55.
9. Chen Q, Shao X, Tian Z, Chen Y, Mondal P, Liu F, et al. Nanoscale monitoring of mitochondria and lysosome interactions for drug screening and discovery. Nano Research. 2019;12(5):1009-15.
10. Chen Q, Shao X, Hao M, Fang H, Guan R, Tian Z, et al. Quantitative analysis of interactive behavior of mitochondria and lysosomes using structured illumination microscopy. Biomaterials. 2020;250:120059.
11. Chen Q, Jin C, Shao X, Guan R, Tian Z, Wang C, et al. Super-Resolution Tracking of Mitochondrial Dynamics with An Iridium(III) Luminophore. Small (Weinheim an der Bergstrasse, Germany). 2018;14(41):e1802166.
12. Bonnay F, Veloso A, Steinmann V, Köcher T, Abdusselamoglu MD, Bajaj S, et al. Oxidative Metabolism Drives Immortalization of Neural Stem Cells during Tumorigenesis. Cell. 2020;182(6):1490-507.e19.
13. Yao CH, Wang R, Wang Y, Kung CP, Weber JD, Patti GJ. Mitochondrial fusion supports increased oxidative phosphorylation during cell proliferation. eLife. 2019;8.
14. Qi X, Qvit N, Su YC, Mochly-Rosen D. A novel Drp1 inhibitor diminishes aberrant mitochondrial fission and neurotoxicity. Journal of cell science. 2013;126(Pt 3):789-802.
15. Szabo A, Sumegi K, Fekete K, Hocsak E, Debreceni B, Setalo G, Jr., et al. Activation of mitochondrial fusion provides a new treatment for mitochondria-related diseases. Biochemical pharmacology. 2018;150:86-96.
16. Abrams AJ, Hufnagel RB, Rebelo A, Zanna C, Patel N, Gonzalez MA, et al. Mutations in SLC25A46, encoding a UGO1-like protein, cause an optic atrophy spectrum disorder. Nature genetics. 2015;47(8):926-32.
17. Baker N, Patel J, Khacho M. Linking mitochondrial dynamics, cristae remodeling and supercomplex formation: How mitochondrial structure can regulate bioenergetics. Mitochondrion. 2019;49:259-68.
18. Quintana-Cabrera R, Mehrotra A, Rigoni G, Soriano ME. Who and how in the regulation of mitochondrial cristae shape and function. Biochemical and biophysical research communications. 2018;500(1):94-101.

19. Pickles S, Vigié P, Youle RJ. Mitophagy and Quality Control Mechanisms in Mitochondrial Maintenance. Current biology : CB. 2018;28(4):R170-r85.
20. Kiriyama Y, Nochi H. Intra- and Intercellular Quality Control Mechanisms of Mitochondria. Cells. 2017;7(1).
21. Bitetto G, Malaguti MC, Ceravolo R, Monfrini E, Straniero L, Morini A, et al. SLC25A46 mutations in patients with Parkinson's Disease and optic atrophy. Parkinsonism & related disorders. 2020;74:1-5.
22. Sesaki H, Jensen RE. UGO1 encodes an outer membrane protein required for mitochondrial fusion. The Journal of cell biology. 2001;152(6):1123-34.
23. Coonrod EM, Karren MA, Shaw JM. Ugo1p is a multipass transmembrane protein with a single carrier domain required for mitochondrial fusion. Traffic (Copenhagen, Denmark). 2007;8(5):500-11.
24. Hammer MB, Ding J, Mochel F, Eleuch-Fayache G, Charles P, Coutelier M, et al. SLC25A46 Mutations Associated with Autosomal Recessive Cerebellar Ataxia in North African Families. Neuro-degenerative diseases. 2017;17(4-5):208-12.
25. Wan J, Steffen J, Yourshaw M, Mamsa H, Andersen E, Rudnik-Schöneborn S, et al. Loss of function of SLC25A46 causes lethal congenital pontocerebellar hypoplasia. Brain : a journal of neurology. 2016;139(11):2877-90.
26. Nguyen M, Boesten I, Hellebrekers DM, Mulder-den Hartog NM, de Coo IF, Smeets HJ, et al. Novel pathogenic SLC25A46 splice-site mutation causes an optic atrophy spectrum disorder. Clinical genetics. 2017;91(1):121-5.
27. Braunisch MC, Gallwitz H, Abicht A, Diebold I, Holinski-Feder E, Van Maldergem L, et al. Extension of the phenotype of biallelic loss-of-function mutations in SLC25A46 to the severe form of pontocerebellar hypoplasia type I. Clinical genetics. 2018;93(2):255-65.
28. Charlesworth G, Balint B, Mencacci NE, Carr L, Wood NW, Bhatia KP. SLC25A46 mutations underlie progressive myoclonic ataxia with optic atrophy and neuropathy. Movement disorders : official journal of the Movement Disorder Society. 2016;31(8):1249-51.
29. van Dijk T, Rudnik-Schöneborn S, Senderek J, Hajmousa G, Mei H, Dusl M, et al. Pontocerebellar hypoplasia with spinal muscular atrophy (PCH1): identification of SLC25A46 mutations in the original Dutch PCH1 family. Brain : a journal of neurology. 2017;140(8):e46.
30. Li Z, Peng Y, Hufnagel RB, Hu YC, Zhao C, Queme LF, et al. Loss of SLC25A46 causes neurodegeneration by affecting mitochondrial dynamics and energy production in mice. Human molecular genetics. 2017;26(19):3776-91.
31. Yang L, Slone J, Li Z, Lou X, Hu YC, Queme LF, et al. Systemic administration of AAV-Slc25a46 mitigates mitochondrial neuropathy in Slc25a46-/- mice. Human molecular genetics. 2020;29(4):649-61.
32. Terzenidou ME, Segklia A, Kano T, Papastefanaki F, Karakostas A, Charalambous M, et al. Novel insights into SLC25A46-related pathologies in a genetic mouse model. PLoS genetics. 2017;13(4):e1006656.

33. Janer A, Prudent J, Paupe V, Fahiminiya S, Majewski J, Sgarioto N, et al. SLC25A46 is required for mitochondrial lipid homeostasis and cristae maintenance and is responsible for Leigh syndrome. EMBO molecular medicine. 2016;8(9):1019-38.
34. Steffen J, Vashisht AA, Wan J, Jen JC, Claypool SM, Wohlschlegel JA, et al. Rapid degradation of mutant SLC25A46 by the ubiquitin-proteasome system results in MFN1/2-mediated hyperfusion of mitochondria. Molecular biology of the cell. 2017;28(5):600-12.
35. Abrams AJ, Fontanesi F, Tan NBL, Buglo E, Campeanu IJ, Rebelo AP, et al. Insights into the genotype-phenotype correlation and molecular function of SLC25A46. Human mutation. 2018;39(12):1995-2007.
36. Chen H, Vermulst M, Wang YE, Chomyn A, Prolla TA, McCaffery JM, et al. Mitochondrial fusion is required for mtDNA stability in skeletal muscle and tolerance of mtDNA mutations. Cell. 2010;141(2):280-9.
37. Sprenger HG, Langer T. The Good and the Bad of Mitochondrial Breakups. Trends in cell biology. 2019;29(11):888-900.
38. Chen H, McCaffery JM, Chan DC. Mitochondrial fusion protects against neurodegeneration in the cerebellum. Cell. 2007;130(3):548-62.
39. Stoldt S, Wenzel D, Kehrein K, Riedel D, Ott M, Jakobs S. Spatial orchestration of mitochondrial translation and OXPHOS complex assembly. Nature cell biology. 2018;20(5):528-34.
40. Kühlbrandt W. Structure and function of mitochondrial membrane protein complexes. BMC biology. 2015;13:89.
41. Stephan T, Brüser C, Deckers M, Steyer AM, Balzarotti F, Barbot M, et al. MICOS assembly controls mitochondrial inner membrane remodeling and crista junction redistribution to mediate cristae formation. The EMBO journal. 2020;39(14):e104105.
42. Harner M, Körner C, Walther D, Mokranjac D, Kaesmacher J, Welsch U, et al. The mitochondrial contact site complex, a determinant of mitochondrial architecture. The EMBO journal. 2011;30(21):4356-70.
43. Ashrafi G, Schwarz TL. The pathways of mitophagy for quality control and clearance of mitochondria. Cell Death & Differentiation. 2013;20(1):31-42.
44. Hamacher-Brady A, Brady NR. Mitophagy programs: mechanisms and physiological implications of mitochondrial targeting by autophagy. Cellular and Molecular Life Sciences. 2016;73(4):775-95.
45. Hytti M, Korhonen E, Hyttinen JMT, Roehrich H, Kaarniranta K, Ferrington DA, et al. Antimycin A-Induced Mitochondrial Damage Causes Human RPE Cell Death despite Activation of Autophagy. Oxidative medicine and cellular longevity. 2019;2019:1583656.
46. Wang H, Zhang T, Ge X, Chen J, Zhao Y, Fu J. Parkin overexpression attenuates Aβ-induced mitochondrial dysfunction in HEK293 cells by restoring impaired mitophagy. Life sciences. 2020;244:117322.

Figures

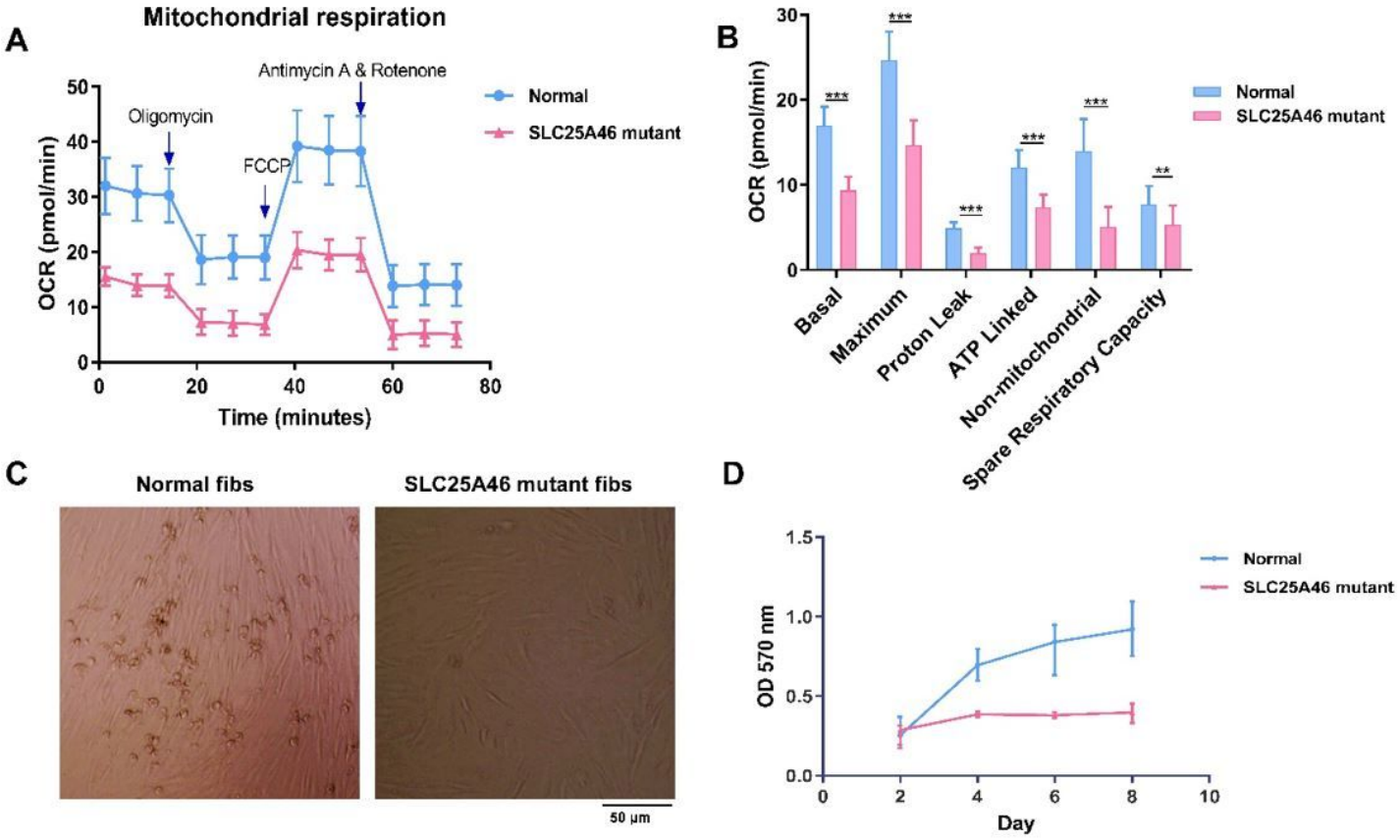

Figure 1

Comparative analysis of mitochondrial respiration and cell proliferation in human-derived normal and SLC25A46 mutant fibroblasts. The oxygen consumption rate (OCR) (a, b) and the cell proliferation rate during one week after the seeding of the cells (c, d) are shown for human-derived normal and SLC25A46 mutant fibroblasts. Data appear as mean ± SD; *** $p < 0.001$, ** $p < 0.01$, as compared to normal fibroblasts.

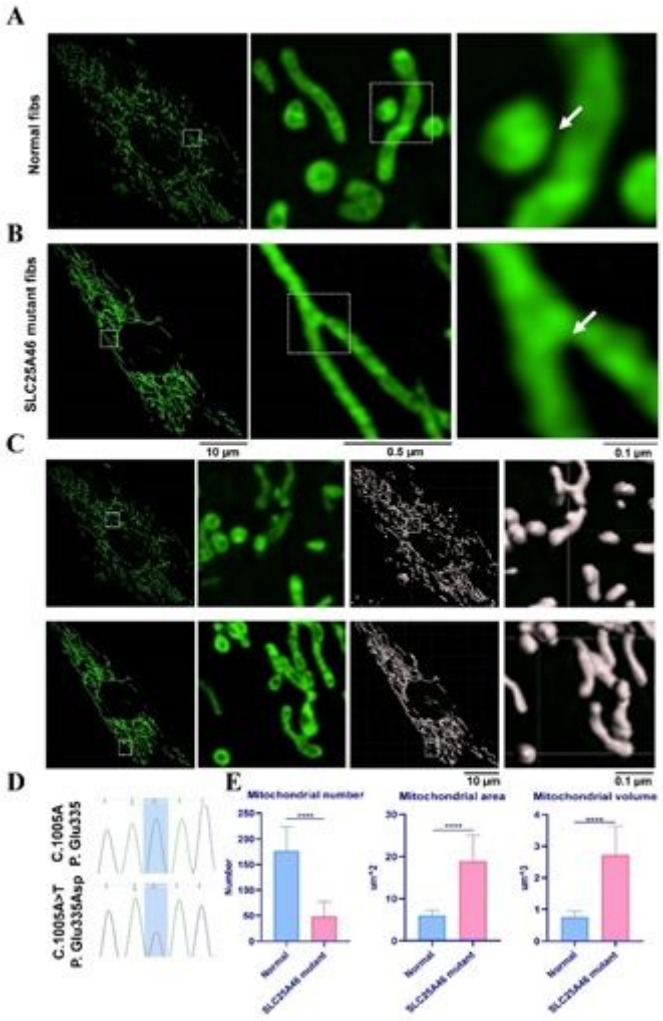

Figure 2

Comparative analysis of mitochondrial morphology in human-derived normal and SLC25A46 mutant fibroblasts. The mitochondrial morphology is shown for human-derived normal (a) and SLC25A46 mutant fibroblasts (b). Quantitative analysis of mitochondrial number was performed by Imaris (c). The Sanger sequencing results of are also shown for the site of the mutant variant for the SLC25A46 cells (d). The results of the quantitative analysis of the mitochondrial area and volume by the Imaris software are also shown (e). Data are presented as mean ± SD (n = 8); **** $p < 0.0001$, as compared to normal fibroblasts.

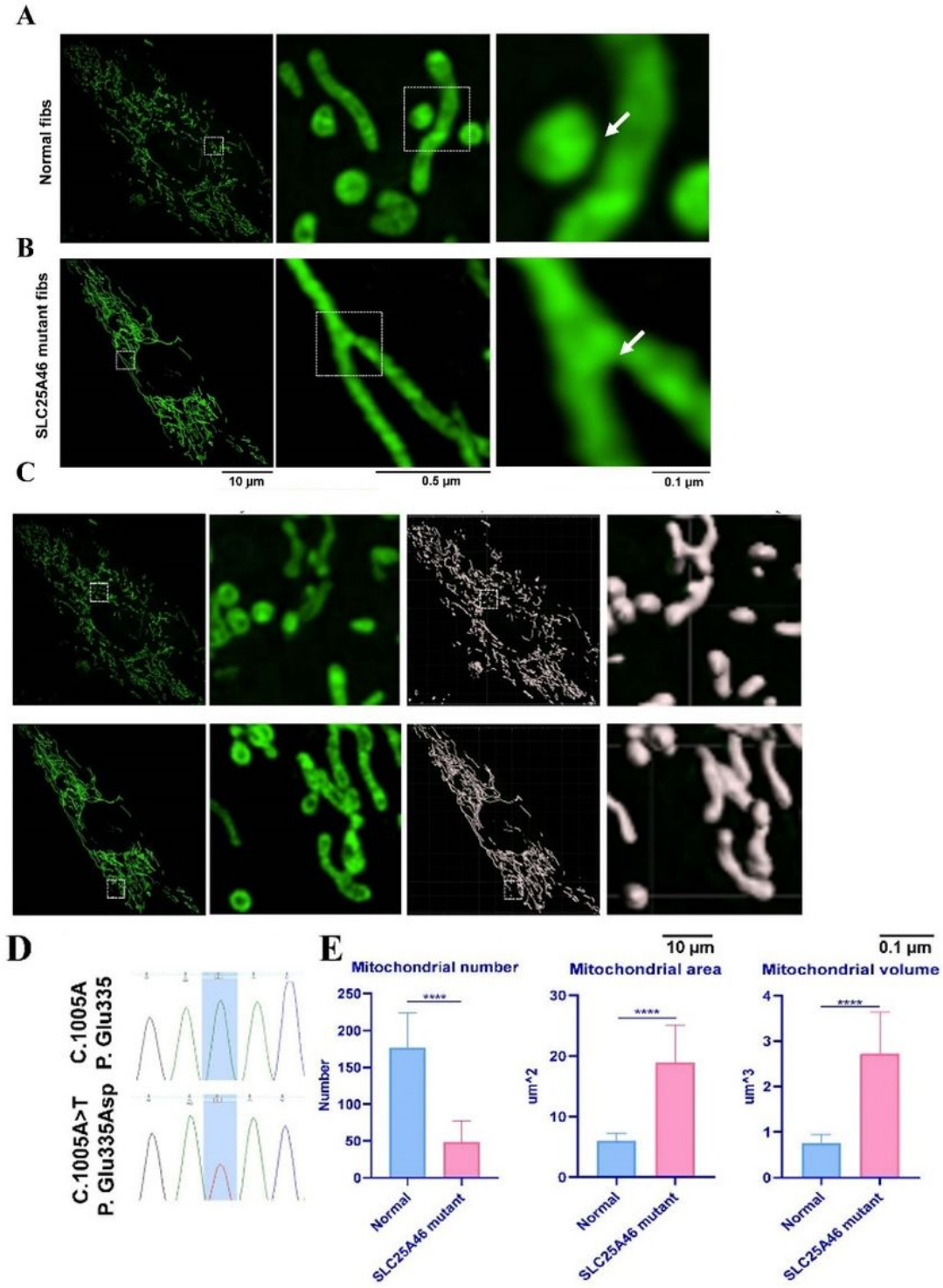

Figure 3

Cristae analysis of mitochondria in human-derived normal and SLC25A46 mutant fibroblasts. Normal cristae (a) were observed in human-derived normal fibroblasts, while invisible cristae and a reduced number and length of cristae (b) were observed in SLC25A46 mutant fibroblasts. Quantification analysis of cristae included the number of cristae per µm (c), cristae length (d), and cristae area (e). Data are present as mean ± SD (n = 8); ** $p < 0.01$, * $p < 0.05$, as compared to normal fibroblasts.

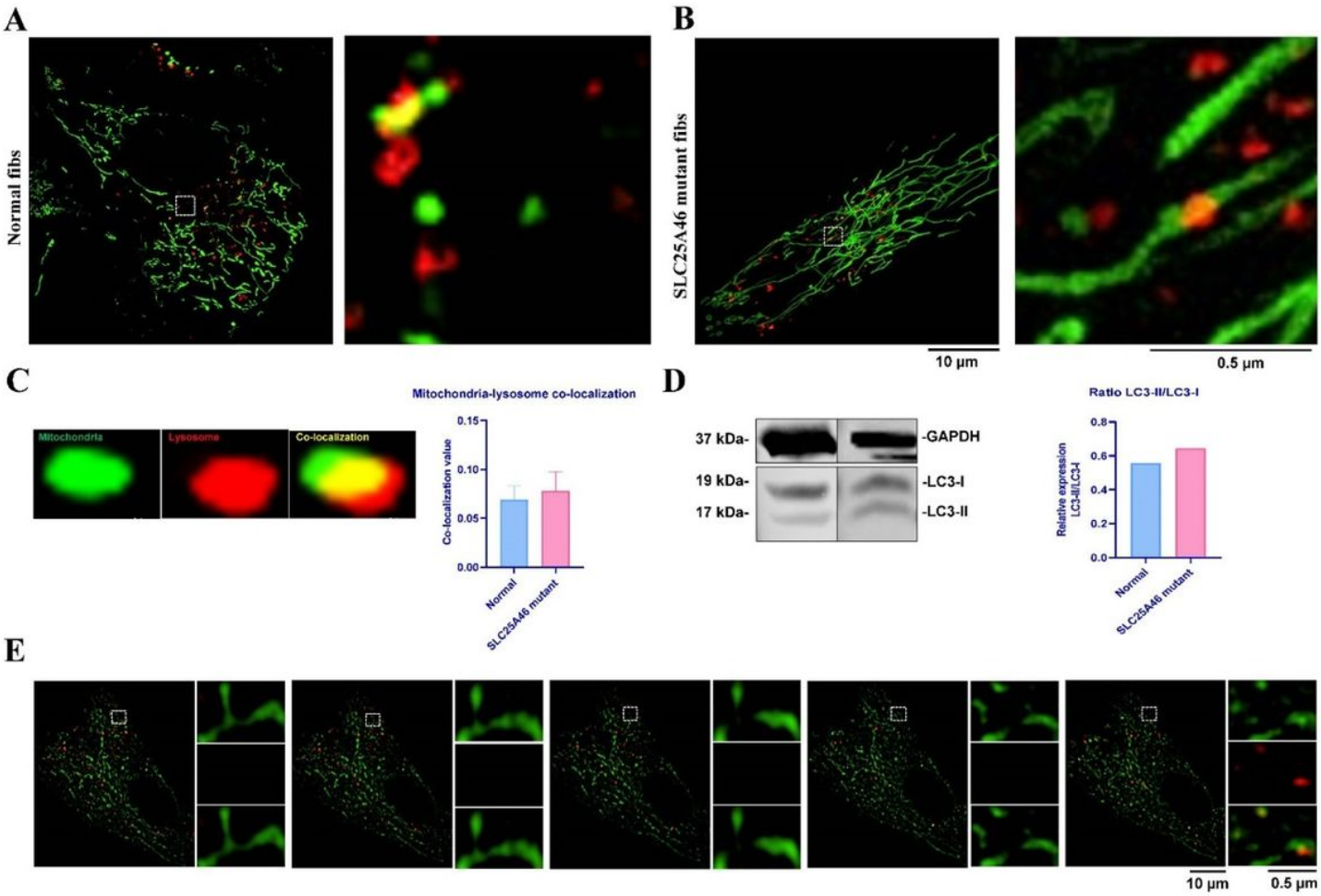

Figure 4

Mitophagy analysis in human-derived normal and SLC25A46 mutant fibroblasts. The same trend of mitophagy is observed in the human-derived normal and SLC25A46 mutant fibroblasts (a, b). This was confirmed by the mitochondria-lysosome co-localization value (c) and Western-blot (d). The mitochondrial dynamics and lysosome-mediated mitophagy could be clearly observed by time-lapse (e).

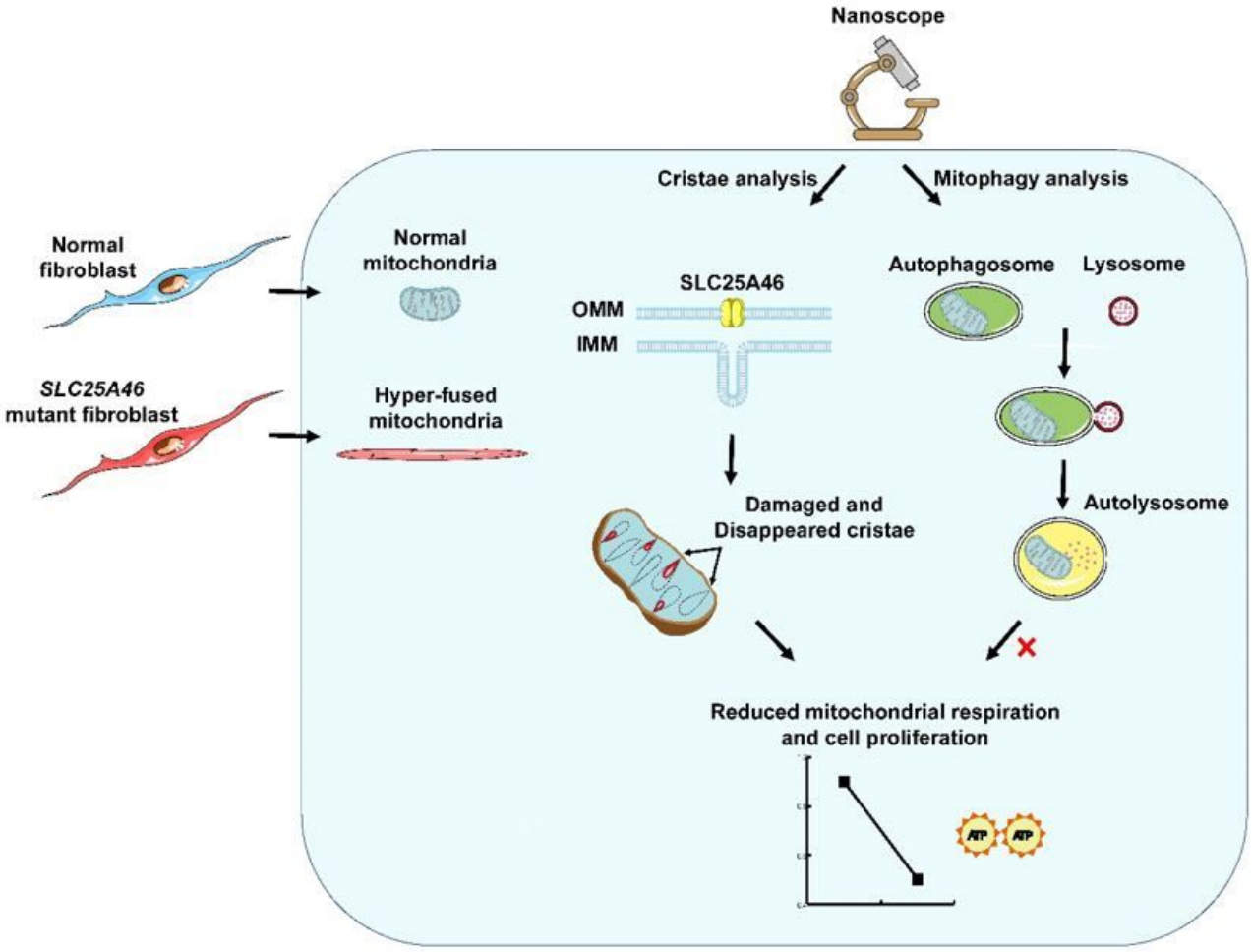

Figure 5

Summary of results for the examination of mitochondrial dysfunction using the nanoscope. The nanoscope can be used to closely analyze the structure of mitochondrial cristae, mitophagy and mitochondrial dynamics in live-cell, which is an extremely suitable application for the clinical analysis of the causes of mitochondrial dysfunction in patients with mitochondrial diseases.